3

Axial segregation in metal-halide lamps under varying gravity conditions during parabolic flights

Abstract.
Metal-halide lamps have high efficiencies. These lamps often contain rare-earth additives (in our case dysprosium iodide) which radiate very efficiently in the visible spectrum. Colour separation is a problem in these lamps; this is caused by axial segregation of these additives as a result of diffusion and convection. To vary the effect of convection, parabolic flights were performed with micro-gravity ($0g$) and hyper-gravity ($\sim 1.8g$) phases. During these flights, the atomic dysprosium density was measured by means of laser absorption spectroscopy. In addition, the lamp voltage and wavelength integrated light output of the lamp, which are strongly influenced by the total amount of Dy in the lamp, were measured. The Dy density, axial segregation and light output are dependent on the gravity. The dynamic lamp behaviour during the parabolas was investigated: the dysprosium density and lamp voltage followed the gravity variations. When entering the micro-gravity phase, the axial diffusion time constant is the slowest time constant; it is proportional to the mercury pressure in the lamp.

This chapter has been adapted from [A.J. Flikweert, M. van Kemenade, T. Nimalasuriya, M. Haverlag, G.M.W. Kroesen and W.W. Stoffels, *Axial segregation in metal-halide lamps under varying gravity conditions during parabolic flights*, J. Phys. D: Appl. Phys. **39** (2006) 1599–1605].

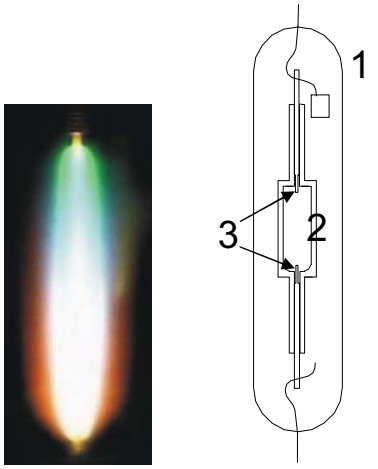

Figure 3.1: (printed in colour in figure 1.3) Left: picture of a MH lamp burner (real size 8 mm x 20 mm); colour separation is clearly visible. Right: schematic picture of the lamp: (1) outer bulb; (2) burner with height 20 mm and diameter 8 mm; (3) electrodes, distance between the both electrodes ∼18 mm.

3.1 Introduction

Metal-halide (MH) lamps, which are high intensity discharge (HID) lamps, have a high efficiency (up to 40%) [3, 21–25]. They contain a buffer gas (mercury) and often rare-earth additives that act as the prime radiator in the visible spectrum. The rare-earth additive is dosed as a salt; the rare-earth vapour above the salt pool is saturated. When burning vertically, the lamp used by us has a non-uniform light output because of segregation of the additives. This colour separation and a schematic picture of the lamp are shown in figure 3.1 [32, 43].

The colour separation [28] is caused by the non-uniform distribution of the rare-earth additives. This distribution originates from convection and diffusion phenomena in the lamp [32, 34, 43, 50]. Convection is caused by gravity and therefore the lamp has been investigated under micro-gravity conditions during parabolic flights and at the International Space Station, where no convection is present in the lamp [41, 51, 52].

To get more insight in the flow phenomena and segregation in the lamp, absorption measurements of atomic dysprosium have been carried out during parabolic flights. During these flights, several parabolas are performed. Each parabola consists of several phases. At the start of a parabola, the gravity is changed from normal ($1g$) to hyper-gravity ($\sim 1.8g$): the airplane pulls up. The next phase is free fall: micro-gravity ($0g$). The final phase is again hyper-gravity. After this parabola, normal gravity returns when flying horizontally.

The dynamic lamp behaviour during the parabolic flights has been investigated [43], the goal being to find a qualitative relationship between the gravity and the Dy density. To understand this dynamic behaviour, one needs a model. The theory propounded by E. Fischer [28] will be used here.

The atomic dysprosium density has been measured at one axial position of the lamp; this gives a measure for axial segregation. Furthermore, the lamp voltage has been measured—this gives a measure for the conductivity of the plasma and the total amount of dysprosium in the plasma. Finally, an integrating sphere has been used to measure the integrated light output by the lamp.

First the theory behind the lamps is introduced. Next the experimental setup is discussed briefly: the lamp, the parabolic flights and the laser absorption technique. The atomic dysprosium density (at a certain axial position) and the lamp voltage are presented for three lamps with varying Hg content during the different phases (normal gravity, hyper-gravity, micro-gravity) of the parabola. Finally, the results obtained by integrated light output measurements are presented.

3.2 Theory

The theory of segregation in infinitely long MH lamps has been propounded by E. Fischer [28]. For our lamp with a limited burner height of 20 mm and diameter of 8 mm and containing DyI_3 as the rare-earth additive, the theory has been described in a prior publication [32]. For the reader's convenience it will be summarized here.

3.2.1 Radial segregation

Because of the large temperature gradient between the wall (∼1200 K) and the centre of the burner (∼5500 K) [29], mainly atoms are present at the centre while at the wall molecules dominate. In addition, at the very centre of the burner, where the temperature is high, Dy atoms are ionized. Due to the different diffusion velocities of atoms, molecules and ions, the light particles in the hotter centre diffuse faster than the heavy molecules near the cooler wall. This results in a hollow radial profile of the total dysprosium concentration (Dy in any chemical form): the so-called radial segregation. Note that this is in addition to the already lower gas density defined by the ideal gas law $p = nkT$. The profiles for the MH lamp have already been presented in literature [32], where the hollow radial profile is clearly seen.

Figure 3.2 shows the total Dy density as a function of the radial position for two situations with an equal amount of Dy in the lamp: in situation B the radial segregation is stronger than in situation A. Note that near the centre dysprosium is mainly present in the form of atoms and ions, whereas at the wall dysprosium is mainly present in the form of molecules. Therefore, for stronger radial segregation, the radially averaged atomic Dy density decreases.

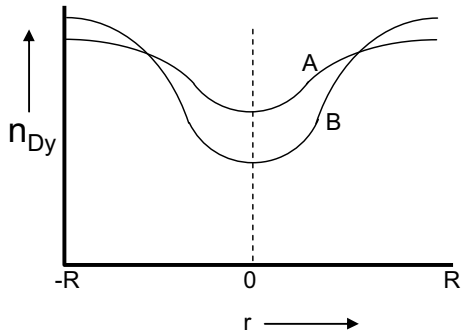

Figure 3.2: Elemental Dy density as a function of radial position. For equal total Dy amounts, in situation B the radial segregation is stronger than in situation A.

At a sufficiently high salt pool temperature, dysprosium is the prime radiator in the lamp. When the amount of Dy increases, the radiation loss is increased. The Dy atoms are responsible for the most of the radiation [41], causing radiation loss at the flanks of the discharge where most of the Dy atoms are present. This results in contraction of the arc. The region around the centre where the temperature is high enough for ionization of Dy becomes smaller. The arc channel, which is the zone where the ionization is high enough for conduction, becomes narrower. Because of the contraction, the resistance of the plasma increases. When the input power P is kept constant, the lamp input voltage depends on the resistance R of the plasma: $V = \sqrt{PR}$. Thus more Dy means a higher resistance R and means therefore a higher voltage V.

3.2.2 Convection and axial segregation

In addition to radial segregation, convection is also present in the lamp: the gas in the hotter centre moves upwards while the gas at the wall moves downwards. As discussed in section 3.2.1, the maximum of the elemental Dy density lies near the wall. Because of this, a net downward flow of Dy results in axial segregation [21, 22]: the atomic Dy density is higher near the bottom of the burner. This has also been shown by earlier measurements on the same type of lamp [32].

E. Fischer [28] predicts for an infinitely long lamp an exponential decrease of the axial atomic Dy density $n_{\mathrm{Dy}}(z)$ with increasing height z in the plasma:

$$n_{\mathrm{Dy}}(z) = n_{\mathrm{Dy},0} \exp\left(-\lambda z\right), \tag{3.1}$$

where the parameter λ is a measure for the axial segregation and $n_{\mathrm{Dy},0}$ is the atomic Dy density at the bottom of the burner.

The axial segregation (colour separation) is a result of the balance between diffusion and convection. Good mixing in the lamp occurs in two limiting cases: when there is

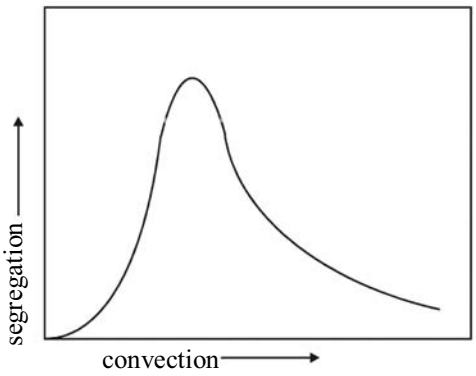

Figure 3.3: The (qualitative) Fischer curve [28]: axial segregation parameter λ of the lamp as a function of the amount of convection. The amount of convection increases with the gravity and is also dependent on the input power and the aspect ratio of the burner. The order of magnitude of λ is 0.20 mm^{-1} [32].

no convection, and when there is extremely high convection. Somewhere in between, the segregation parameter λ has a maximum. The convection increases among other things with the gravity. The Fischer curve (segregation parameter as a function of gravity) is shown in figure 3.3.

In figure 3.4 the dysprosium density distribution over the length of the lamp is shown schematically for various values of the axial segregation parameter λ. When measuring the dysprosium density at a particular axial position, the density varies with the amount of segregation. The density at the lower electrode (near the cold spot) is constant for a fixed temperature. When no axial segregation is present (situation A), one measures a higher density than when the lamp shows strong axial segregation (situation C).

3.2.3 Convection time constants

In order to understand the dynamic lamp behaviour when turning the gravity 'off', in our case switching from hyper-gravity to zero gravity during parabolic flights (section 3.1), we estimate several typical time constants in the lamp. The three time constants that are estimated are the convection time constant, the radial diffusion time constant and the axial diffusion time constant.

The convection in the lamp is driven by gravity. When switching to micro-gravity at $t = 0$ s, the driving force of the convection flow disappears. The present kinetic energy of the convective flow is dissipated by viscous dissipation [53]. The kinetic energy per unit volume is equal to $\frac{1}{2}\rho v^2$, whereas the viscous dissipation per unit volume and per

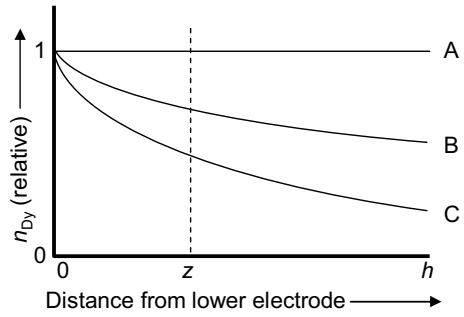

Figure 3.4: The radially integrated total Dy density (in any chemical form) as a function of the axial position in the lamp burner (bottom at 0 and top at h), for different values for the axial segregation parameter λ (infinitely long lamp). At situation A no axial segregation is present, whereas at situation C strong axial segregation is present. When the Dy density at the lower electrode is fixed (normalized to 1), the total Dy density measured at the dashed position z is a measure of the axial segregation parameter λ.

unit time is given by $\mu \cdot (\frac{\mathrm{d}v}{\mathrm{d}r})^2$. In these expressions, v is the flow velocity, r is the radial position, μ is the dynamic viscosity (kg m^{-1} s^{-1}) and ρ is the density of the bulk gas in the burner (mercury in our case). For the total energy dissipated by viscous dissipation, one has to integrate the viscous dissipation (per unit volume and per unit time) over time.

It is assumed that the flow velocity decays exponentially from $t = 0$ s:

$$v(r,t) = \begin{cases} v_0(r) & \text{for} \quad t < 0 \\ v_0(r) \exp\left(-\frac{t}{\tau_{\mathrm{conv}}}\right) & \text{for} \quad t \geq 0 \end{cases}, \tag{3.2}$$

where τ_{conv} is a measure for the time the convection flow persists after switching off the gravity. By setting the kinetic energy and the viscous dissipation (integrated over time) equal and using equation (3.2), one gets for the convection time constant τ_{conv}:

$$\frac{1}{2}\rho v_0^2(r) = \int_{t=0}^{\infty} \mu \left(\frac{\mathrm{d}v_0(r)}{\mathrm{d}r}\right)^2 \exp\left(-\frac{2t}{\tau_{\mathrm{conv}}}\right) \mathrm{d}t \Leftrightarrow \tau_{\mathrm{conv}} = \frac{\rho v_0^2}{\mu \left(\mathrm{d}v_0(r)/\mathrm{d}r\right)^2}. \tag{3.3}$$

The convection speed at the axis of the lamp is about 0.20 m s^{-1} and near the wall -0.06 m s^{-1} [54]. When the ratio $v(r)/\left(\mathrm{d}v/\mathrm{d}r\right)$ is assumed to be constant under different conditions (gravity, pressure, input power), for our conditions (table 3.1) this results in convection time constants of less than 1 s as given in table 3.2.

Table 3.1: Values used for calculating time constants.

R_{burner}	4.0 mm
l_{burner}	20.0 mm
T_{eff}	3000 K [53]
n (5 mg Hg)	1.50×10^{25} m^{-3}
n (7.5 mg Hg)	2.25×10^{25} m^{-3}
n (10 mg Hg)	1.50×10^{25} m^{-3}

Table 3.2: Convection time constants for different amounts of Hg.

mg Hg	τ_{conv} (s)
5.0	0.07
7.5	0.11
10.0	0.14

3.2.4 Diffusion time constants

Two other time constants are the radial diffusion time constant and the axial diffusion time constant. For the diffusion time of a particle only the collisions with the bulk (mercury) are regarded. The diffusion time τ_{diff} is given by [55]

$$\tau_{\text{diff}} = \frac{l^2}{D}, \tag{3.4}$$

with l the typical length scale. For radial segregation this is approximately the radius ($l = R$), whereas for axial segregation the height of the burner is taken ($l = h$). The diffusion coefficient D is estimated by (hard-sphere scattering) [55]

$$D = \frac{k_b T_{\text{eff}}}{m_{\text{r}} \nu}. \tag{3.5}$$

Here k_b is the Boltzmann constant, T_{eff} is the effective temperature, m_{r} is the reduced mass (of mercury and the particle) and ν is the collision frequency of the particle and Hg.

Using the values in table 3.1 and the effective radii of the particles in table 3.3, the diffusion time constants are calculated and presented in table 3.4.

Another time constant may be the warming up of the burner when varying the gravity. The burner consists of quartz of 1 mm thickness; its heat capacity is 1.4 J K^{-1} [57]. With a rough estimate of a 100 K temperature change and taking 50% of the input power for heating the burner, one obtains a warming-up time of $\sim$2 s. The real time constant is probably (much) smaller (lower temperature change), so the warming-up time constant is ignored.

Table 3.3: Effective particle radii for calculating time constants [56].

Species	Radius ($\times 10^{-10}$ m)
Dy	2.23
DyI	3.50
DyI_2	4.25
DyI_3	4.63
Dy_2I_6	5.50
Hg	2.09

Table 3.4: Diffusion time constants along radius and axis for several particles.

	mg Hg	Dy (s)	DyI (s)	DyI_2 (s)	DyI_3 (s)	Dy_2I_6 (s)
Along	5.0	0.34	0.68	1.00	1.22	1.80
the	7.5	0.52	1.03	1.51	1.83	2.70
radius	10	0.69	1.37	2.01	2.44	3.60
Along	5.0	8.6	17.1	25.1	30.5	45.0
the	7.5	12.9	25.6	37.7	45.8	67.5
axis	10	17.2	34.2	50.2	61.1	90.1

The convection time constants are much smaller than the axial diffusion time constants. This means that when entering the micro-gravity phase from the hyper-gravity phase, the convection flow disappears fast and the speed of stabilization of the dysprosium distribution is determined by the axial diffusion time constant. This time constant is proportional to the mercury pressure.

3.3 Experimental setup

3.3.1 The lamp

The lamp that is measured contains Hg as buffer gas, 300 mbar Ar/Kr^{85} as a starting gas and 4.2 mg DyI_3 as a salt additive. A schematic picture of the lamp is shown in figure 3.1. The amount of Hg is varied; lamps with 5, 7.5 and 10 mg of Hg are measured. The ballast (Philips HID-DynaVision LA 0307, square wave of 125 Hz) delivers a constant power of 150 W. The lamp voltage is read out by the ballast.

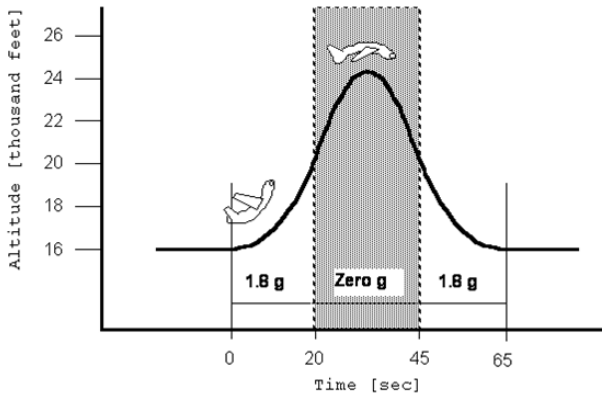

Figure 3.5: Parabolic sequence: hyper-gravity (∼20 s), micro-gravity (the main phase, ∼25 s) and again hyper-gravity (∼20 s).

3.3.2 Parabolic flights

The lamp was measured under micro-gravity conditions during the parabolic-flight campaign of the European Space Agency (ESA) in June 2004 [40]. During each flight, 31 parabolas were performed. In figure 3.5 the height of the airplane and the gravity are shown schematically. Each parabola starts with hyper-gravity: the pull-up phase. The second phase is the injection phase. In this phase of about 25 s all forces are compensated: zero gravity is achieved. The last phase of the parabola is a hyper-gravity phase where the airplane pulls out of the free fall.

In figure 3.6 an example is given of the effective g forces during one parabola. As is seen in this figure, the hyper-gravity phases are not well defined. The micro-gravity phases are controlled very well; therefore we will focus on the micro-gravity phases.

3.3.3 Laser absorption spectroscopy

To get insight into the axial segregation, we measured the radially averaged density of ground state dysprosium using laser absorption spectroscopy. The measurement technique has been described in detail in section 2.3 [32].

A tunable diode laser (Sacher TEC 500 645-5, typical line width ≤ 3 fm) scans a small wavelength range (0.17 nm) around the absorption wavelength $\lambda = 642.19$ nm. The transition probability of this transition is 1.615×10^5 s^{-1} [44, 45]. This line is pressure broadened with a width of around 40 pm (experimentally determined).

In figure 3.7 a schematic overview of the setup for the laser absorption measurements on the lamp is given. The laser beam (height ∼1 mm) is transformed to a parallel sheet

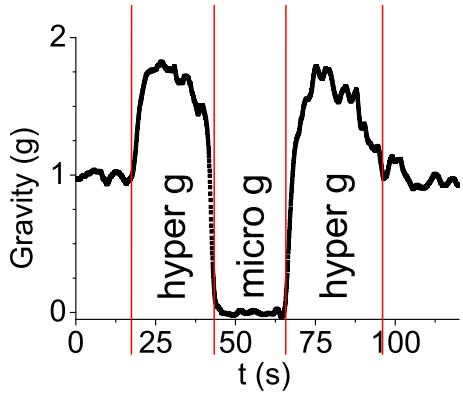

Figure 3.6: Gravity as a function of time during one parabola; the start of the time axis is chosen arbitrary. The micro-gravity and hyper-gravity phases are indicated.

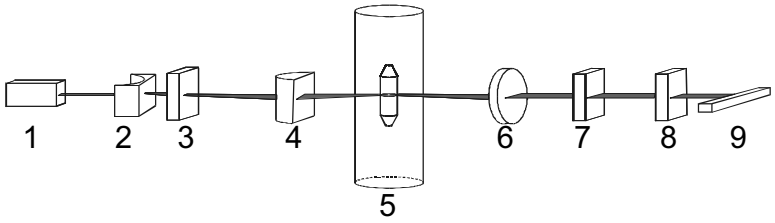

Figure 3.7: Schematic overview of the absorption setup used to measure the ground state Dy density in a MH lamp: (1) diode laser; (2) cylindrical lens, $f = -12.7$ mm; (3) cylindrical lens, $f = +62.9$ mm; (4) lamp; (5) spherical lens, $f = +100$ mm; (6) interference filter; (7) diode array.

inside the lamp burner by two cylindrical lenses. After the beam passes the plasma, it converges to a parallel beam, then passes an interference filter and hits the diode array (32 evenly spaced photodiodes). Each detector channel is converted into a lateral position x; in this way a lateral absorption profile is obtained.

The measurement method is shown in figure 3.8. For each lateral position the laser intensity is measured for lamp-off and lamp-on (corrected for dark current). The indicated lamp emission is independent of the laser wavelength. From these curves the absorption and subsequently the line-of-sight dysprosium density are calculated. Finally the data are converted into a radially averaged dysprosium density profile n_{Dy} [29, 32, 48, 49].

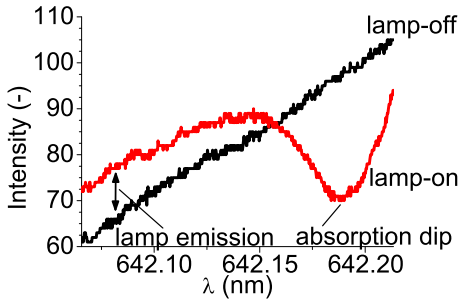

Figure 3.8: Measured laser intensity as a function of wavelength λ at a particular lateral position for lamp-on and lamp-off. The absorption dip (at 642.19 nm) and lamp emission are indicated. The intensity is given in arbitrary units.

3.3.4 Integrated light emission setup

In order to measure the total lamp emission, the lamps are placed in an integrating sphere, which collects and homogenizes the total light output of the lamp [51]. This light is then detected by a photodiode supplied with a suitable optical filter, simulating human eye sensitivity.

The integrating sphere measurements have been carried out on the same lamps as the Dy density and voltage measurements, but at a different parabolic flight campaign.

3.4 Results

Three different lamps were measured during parabolic flights. The amounts of mercury are different, 5, 7.5 and 10 mg, which correspond to 6, 9 and 12 bar, respectively, for $T_{\text{eff}} = 3000$ K (Table 3.1).[1] The radially averaged ground state atomic dysprosium density was measured at 5 mm above the lower electrode. At the same time, the lamp voltage was measured. The measurements of the Dy density and lamp voltage are presented. Next, the results of the integrated light emission measurements are presented. The time constant when entering the micro-gravity phase is presented and discussed.

The atomic Dy density, lamp voltage, gravity and wavelength integrated light output during a parabola are shown in figures 3.9–3.13; the start of the time scale was chosen arbitrary during a $1g$ phase. The Dy density and lamp voltage have been normalized: the density and voltage have been set to unity at $1g$. In the graphs, the micro-gravity phase and hyper-gravity phases are indicated. At normal gravity, the

[1] When the cold zones behind the electrodes are taken into account, the pressures are around 5, 7.5 and 10 bar respectively.

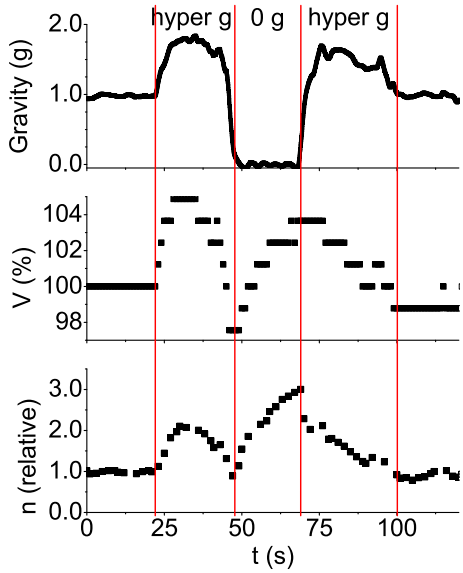

Figure 3.9: Radially averaged Dy density, lamp voltage and gravity as functions of time at 5 mg Hg (6 bar).

order of magnitude of the atomic Dy density was $\sim 10^{21}$ m^{-3} and the lamp voltage was ∼80 V, ∼100 V and ∼120 V for 5 mg, 7.5 mg and 10 mg Hg, respectively.

It was observed that the Dy density varies with gravity. In the hyper-gravity phase, the measured (integrated) Dy density increased. When switching from hyper-gravity to micro-gravity the Dy density decreased rapidly (∼1 s) followed by a slow density increase. In the second hyper-gravity phase, the density increased again.

The lamp voltage is a measure for the total amount of dysprosium in the gas phase in the lamp and thus of the degree of axial segregation in the lamp, as explained in section 3.2.1. This was also observed in figure 3.9–3.11: the lamp voltage follows the same trend as the Dy density.

The integrated light emission in figures 3.12 and 3.13 follows the trends in the radially averaged Dy density and the voltage over the lamp closely. The integrating sphere measurements have been carried out on the same lamps as the absorption and voltage measurements, but at a different parabolic flight campaign. This means that the measurements on the same lamp are reproducible.

The increase in Dy density and the increased light emission at the first hyper-gravity phase can be understood by a better mixing (right-hand side of the Fischer curve (figure 3.3) and thus less axial segregation (situation C to B in figure 3.4) and increasing the total amount of radiating Dy in the arc. The positions in the Fischer curve correspond

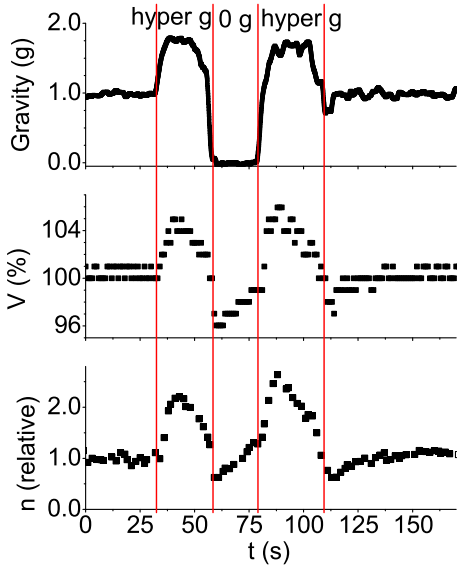

Figure 3.10: Radially averaged Dy density, lamp voltage and gravity as functions of time at 7.5 mg Hg (9 bar).

to those observed in other measurements on the same type of lamp [32, 41].

The gravity data in figures 3.9–3.11 show that only the micro-gravity phase is well defined. During the hyper-gravity phases, the gravity was not constant. Note that the Dy density and lamp voltage closely followed the gravity variations; an example is shown in figure 3.11. A higher gravity means a higher Dy density and thus less axial segregation. This means that above $1g$ we are at the right-hand side of the maximum in the Fischer curve (figure 3.3).

When switching from hyper-gravity to micro-gravity, one observes a steep decline in the Dy density. Several time constants play a role right after entering the micro-gravity phase (sections 3.2.3 and 3.2.4); the convection time constant is the smallest ($\sim$0.1 s) and the axial diffusion time constant is the largest ($\sim$30 s). The radial diffusion time constant is $\sim$1 s. When the micro-gravity phase is entered, the radial segregation increases. The total amount of dysprosium (in any chemical form) remains more or less constant due to the fact that the axial diffusion is slow compared to the radial diffusion time constants. Atoms are mainly present around the hot centre (section 3.2.1), so more radial segregation means fewer Dy atoms around the centre and (slightly) more DyI_x molecules near the wall. Only atoms have been measured, so the radially averaged Dy density decreases.

During the micro-gravity phase, the density was increasing because the axial se-

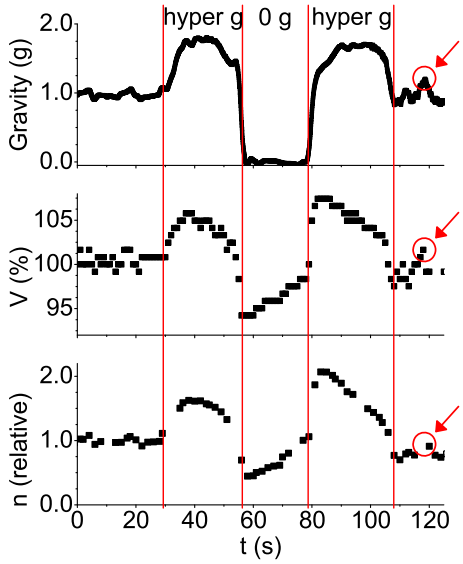

Figure 3.11: Radially averaged Dy density, lamp voltage and gravity as functions of time at 10 mg Hg (12 bar). The Dy density and lamp voltage closely follow the gravity variations; an example is indicated by the circles.

gregation tended to disappear (towards situation A in figure 3.4; left-hand side of the Fischer curve in figure 3.3). The total amount of atomic dysprosium also increases with decreasing axial segregation (the area under the curves shown in figure 3.4). This also explains the increased light output observed in figures 3.12 and 3.13.

The micro-gravity phase is the only well-defined phase of the parabola; therefore only at this part (rising Dy density) has the time constant been fitted. The time constants were determined from figures 3.9–3.11; here a linear fit was applied. In figure 3.14 the results are plotted for the three different lamps. The trend and the order of magnitude of the time constants correspond to the values presented in table 3.4.

At the end of the micro-gravity phase, the lamp was still not in equilibrium: especially for 7.5 and 10 mg Hg the time constants are greater than the duration of the micro-gravity phase (∼20 s). Therefore the lamps have also been investigated in space in the International Space Station (ISS) [41].

When switched from the micro-gravity phase to the second hyper-gravity phase, a steep increase was observed. The atomic Dy density at the end of the micro-gravity phase is determined by the Hg pressure and the axial diffusion time constant. In the second hyper-gravity phase the new equilibrium was reached fast (convection time constant ~ 0.1 s); the Dy density was again higher than for normal gravity, due to less

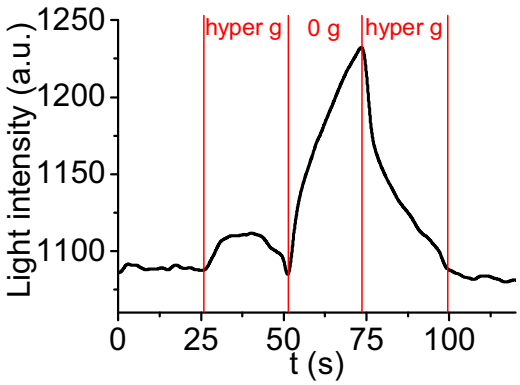

Figure 3.12: Integrated light emission of the lamp burning in vertical position with 5 mg Hg (6 bar) at 150 W as a function of time during one parabola [58]. The trend is similar to the density and voltage measurements presented in figure 3.9.

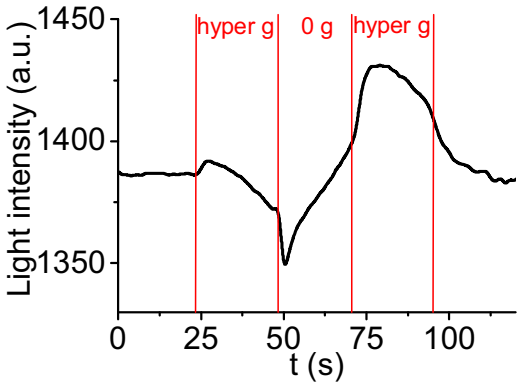

Figure 3.13: Integrated light emission of the lamp burning in vertical position with 10 mg Hg (12 bar) at 150 W as a function of time during one parabola [58]. The trend is similar to the density and voltage measurements presented in figure 3.11.

radial segregation and an overall higher Dy density in the lamp.

3.5 Conclusions

The dynamic behaviour of three lamps during parabolic flights (different amounts of mercury) was investigated. The radially averaged atomic dysprosium density was mea-

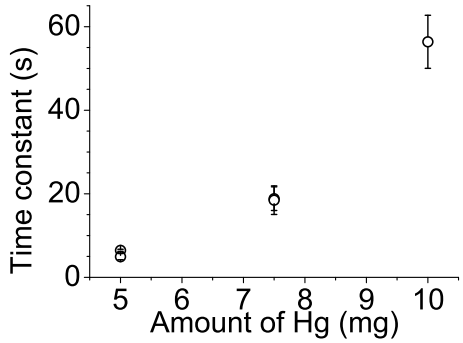

Figure 3.14: Time constants at the micro-gravity phase for different amounts of Hg; 5, 7.5 and 10 mg Hg correspond to 6, 9 and 12 bar, respectively.

sured by means of laser absorption spectroscopy. Furthermore the lamp voltage was measured, which turns out to be a measure for the total amount of dysprosium in the lamp.

By changing the gravity, the amount of convection was varied. The axial segregation is inversely proportional to the measured atomic dysprosium density. The lamps follow the qualitative description presented by E. Fischer.

Three processes with different time constants play a role when switching from hyper-gravity to micro-gravity. The axial diffusion time constant is the slowest time constant ($\sim$30 s), which is proportional to the amount of mercury, as predicted by the theory. As a result, at the end of the micro-gravity phase the lamp is still not in equilibrium. Therefore the lamps have also been tested in the ISS.

The total light output of a metal-halide lamp strongly depends on the gravity conditions. The light emission decreases when the axial segregation increases. The results for the integrated light emission measurements are in agreement with the Dy density measurements performed by laser absorption spectroscopy and the lamp voltage measurements.

Acknowledgments

The authors are grateful to all participants in the ARGES project for their contributions, ESA [40] and Novespace [59] for the parabolic flight campaigns and the g level data, and Senter-Novem (project EDI 03146) and the Dutch Ministries of Research and Education as well as Economic Affairs for funding the research.